Spatiotemporal control of spindle midzone formation by PRC1 in human cells

Changjun Zhu, Eric Lau, Robert Schwarzenbacher, Ella Bossy-Wetzel, and Wei Jiang†

The Burnham Institute for Medical Research, 10901 North Torrey Pines Road, La Jolla, CA 92037

Edited by Tony Hunter, The Salk Institute for Biological Studies, La Jolla, CA, and approved March 1, 2006 (received for review August 10, 2005)

We have examined the role of PRC1, a midzone-associated, microtubule bundling, Cdk substrate protein, in regulating the spatiotemporal formation of the midzone in HeLa cells. Cdk-mediated phosphorylation of PRC1 in early mitosis holds PRC1 in an inactive monomeric state. During the metaphase-to-anaphase transition, PRC1 is dephosphorylated, promoting PRC1 oligomerization. Using time-lapse video microscopy, RNA interference, 3D immunofluorescence reconstruction imaging, and rescue experiments, we demonstrate that the dephosphorylated form of PRC1 is essential for bundling antiparallel, nonkinetochore, interdigitating microtubules to establish the midzone that is necessary for cytokinesis. Our results thus indicate that PRC1 is an essential factor in controlling the spatiotemporal formation of the midzone in human cells.

Cdk phosphorylation | mitosis/cytokinesis | microtubule-associated proteins | microtubule bundling

During the metaphase-to-anaphase transition, a conspicuous network of antiparallel nonkinetochore interdigitating microtubules (MTs) assembles between separating chromosomes. This unique structure is referred to as the spindle midzone. The midzone is believed to be required for the maintenance of overall spindle architecture, spindle elongation, and cleavage furrow positioning (1, 2). Previous studies indicated that the midzone-associated centralspindlin complex might play a crucial role in regulating midzone formation. The complex exists as a heterotetramer comprising the midzone-associated kinesin motor, MKLP1, and its binding protein, MgcRacGAP (a Rho-family GTPase activating protein) (3). The heterotetramer, but not the individual MKLP1 or MgcRacGAP proteins, has MT bundling activity (3). Cdk (Cdc2/cyclin B) phosphorylates MKLP1 and negatively regulates its motor and MT-bundling activities (4). Because inactivation of Cdk activity (through the destruction of cyclin B) is critical for the metaphase-to-anaphase transition, it was suggested that Cdk phosphorylation of MPLK1 controls the timing of midzone formation (4, 5). However, recent studies indicate that MKLP1 is not directly involved in the early stages of midzone formation in mammalian cells (6, 7). Immunofluorescence and time-lapse live cell imaging analyses revealed that inhibition of MKLP1 expression does not perturb the bundling of midzone interdigitating MTs. Instead, it inhibits midbody formation and the completion of cytokinesis. Thus, the centralspindlin complex is required for constricting the midzone and forming the midbody that is essential for completing cytokinesis in mammalian cells (7).

PRC1 originally was identified as a Cdk substrate in an *in vitro* phosphorylation screen and was subsequently shown to be a midzone-associated protein required for cytokinesis (8). PRC1 forms oligomers *in vivo* and has MT-binding and -bundling activities (8, 9). Cdk phosphorylation of PRC1 appears to be important for suppressing PRC1 MT-bundling activity in early mitosis, because a Cdk-nonphosphorylatable mutant of PRC1 causes extensive bundling of the metaphase spindle (9). Perturbing the function of PRC1 or PRC1-related orthologs in various species (Ase1p in yeast, SPD-1 in *Caenorhabditis elegans*, AtMAP65 in *Arabidopsis*, and Feo in *Drosophila*) inhibits the formation of midzone interdigitating MT bundles, resulting in two disarrayed half spindles (9–15). The centralspindlin complex, chromosomal passenger proteins, and other midzone-associated proteins mislocalize in PRC1-depleted anaphase cells (refs. 16 and 17; C.Z. and W.J., unpublished results). In addition, PRC1 specifically interacts with the kinesin motor protein, Kif4 (16, 18). During the metaphase-to-anaphase transition, Kif4 translocates PRC1 along MTs to the plus ends of interdigitating mitotic spindles, and the timing of this translocation is controlled by Cdk phosphorylation of PRC1 (18). PRC1 is thus a good candidate for bundling interdigitating MTs to form the midzone. In this article, we determine the molecular mechanism by which PRC1 regulates the spatiotemporal formation of the midzone in HeLa cells.

Results and Discussion

The Predicted Molecular Structure of PRC1. Previous studies showed that the MT-binding domain of PRC1 was mapped in the central region of PRC1, whereas its Cdk phosphorylation sites (Thr-470 and Thr-481) were located at the junction between the MT-binding domain and the C-terminal region of the molecule (8, 9). Because the oligomerization domain of PRC1 had not been defined, mammalian expression constructs expressing FLAG-tagged PRC1, Myc-tagged PRC1, and a series of Myc-tagged PRC1 deletion mutants were generated, and combinations of the corresponding proteins were coexpressed in HeLa cells. Coimmunoprecipitation analyses indicated that PRC1 requires its N terminus (amino acids 1–184) for oligomerization (Fig. 5, which is published as supporting information on the PNAS web site). Hence, PRC1 has an N-terminal oligomerization domain, a central MT-binding domain, and two Cdk phosphorylation sites at the junction between the MT-binding domain and the C-terminal region (Fig. 6*A*, which is published as supporting information on the PNAS web site).

Despite many attempts, we failed to crystallize PRC1 to determine the atomic tertiary structure of PRC1. Therefore, we analyzed PRC1 secondary structure by using the profile-profile alignment algorithm Fold and Function Assignment System (FFAS) (19). Consistent with our previous primary sequence prediction (8, 9), FFAS analysis indicated that the N-terminal two thirds of PRC1 (amino acids 1–465) has significant helical secondary structure, similar to a number of helical proteins like colicin E3, spectrin alpha chain, and vinculin. The C-terminal region of PRC1 (amino acids 466–620), which contains the two Cdk phosphorylation sites (Thr-470 and Thr-481), has mostly β-sheets and -turns with low complexities. The atomic tertiary structure of colicin E has been resolved (20), and we therefore modeled the tertiary structure of PRC1 based on the 1CII.pdb coordinates of colicin E by using SWISSMODEL (Fig. 6*B*; see also Movie 1, which is published as supporting information on the PNAS web site). PRC1 was predicted to form a "g"-shaped tertiary structure. The N-terminal oligomerization domain of PRC1 was predicted to form a three antiparallel α-helical bundle that is likely to mediate protein–

Conflict of interest statement: No conflicts declared.

This paper was submitted directly (Track II) to the PNAS office.

Abbreviations: ECFP, enhanced cyan fluorescent protein; EYFP, enhanced yellow fluorescent protein; MT, microtubule; siRNA, small interfering RNA.

†To whom correspondence should be addressed. E-mail: wjiang@burnham.org.

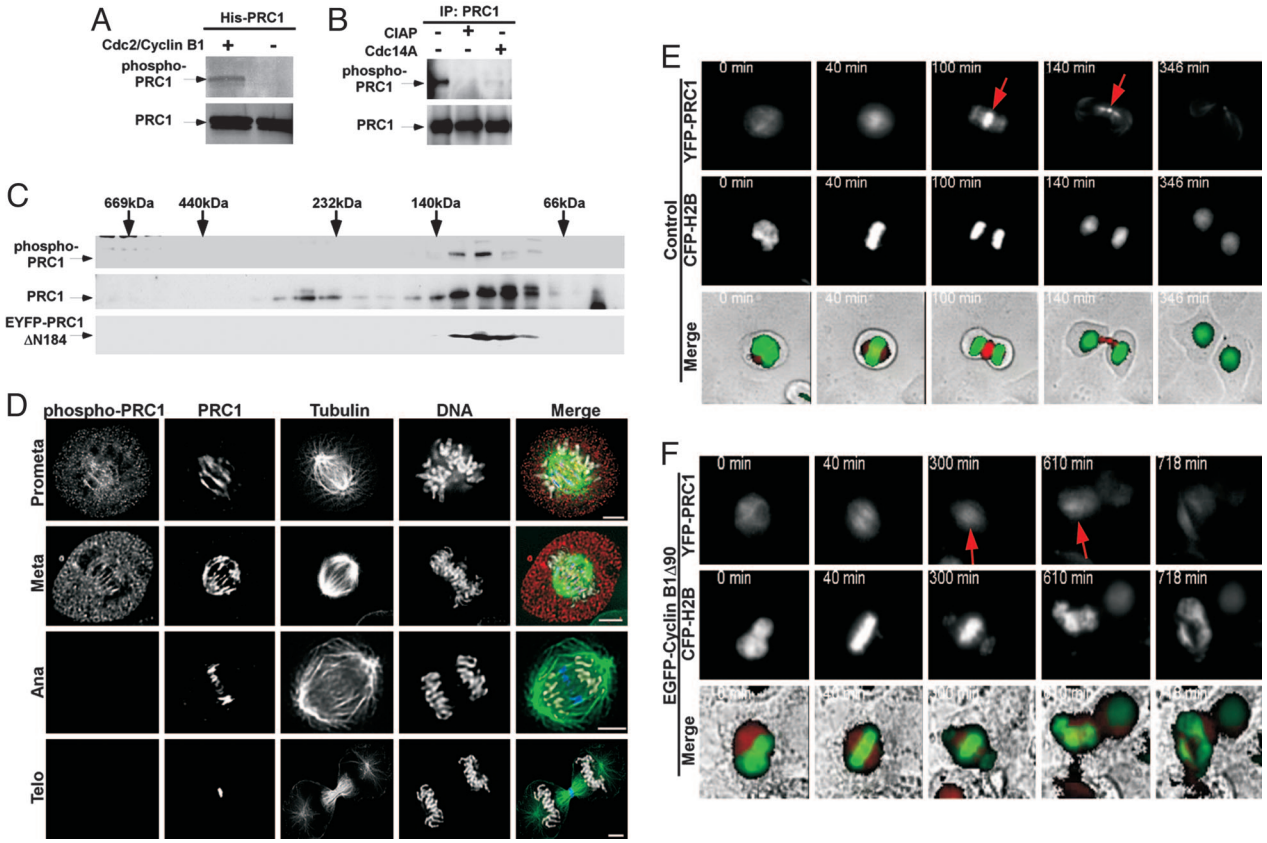

Fig. 1. Effects of Cdk phosphorylation on PRC1 oligomerization and spindle localization. (*A*) Purified, bacterially expressed, His-tagged PRC1 was incubated with or without baculovirus-expressed, purified Cdc2/cyclin B1 in the presence of ATP. The reactions were subjected to immunoblotting analysis by using α-PRC1 or α-PRC1P. (*B*) Mitotic HeLa cell lysates were incubated with α-PRC1 antibody, and the immunoprecipitates then were incubated with or without phosphatases (GST-Cdc14A or CIAP). The reactions were subjected to immunoblotting analysis by using α-PRC1 or α-PRC1P. (*C*) HeLa cells or HeLa cells expressing EYFP-PRC1ΔN184 were lysed in 1% Nonidet P-40 lysis buffer, and cell lysates were subjected to sucrose gradient sedimentation (5% to ≈30%) by ultracentrifugation. The sediments were collected and subjected to immunoblotting analysis by using α-PRC1, α-PRC1P, or anti-GFP antibody. (*D*) Asynchronous HeLa cells grown on coverslips were fixed with 3% formaldehyde and then stained with α-PRC1P (red), α-PRC1 (blue), anti-α-tubulin antibody (green), and DAPI (DNA, white). (Scale bars: 5 μm.) (*E* and *F*) HeLa cells grown on 35-mm glass-bottom dishes were transfected with 0.5 μg of pEYFP-PRC1 and 0.5 μg of pECFP-H2B together with (*F*) or without (*E*) 0.1 μg of pEGFP-cyclin B1Δ90. Thirty-six hours after transfection, cells were placed on a 37°C heated stage, and time-lapse images were collected under a Zeiss Axiovert 100M inverted fluorescence microscope at 2-min intervals by using an automatic digital charge-coupled device camera for 9–10 h. The movies were edited by using SLIDEBOOK 3.0 and DIRECTOR MX (Adobe Systems, San Jose, CA). Representative images of the movies are shown (EYFP-PRC1, pseudocolored red; ECFP-H2B, pseudocolored green). Red arrows indicate spindle midzone/midbody localization of PRC1 in control cells and abnormal mitotic spindle localization of PRC1 in pEGFP-cyclin B1Δ90-transfected cells.

protein interaction (e.g., oligomerization). The central MT-binding domain of PRC1 was predicted to form two long antiparallel α-helixes, connected by a low-complexity structure with β-sheets and -turns that might mediate PRC1 and MT binding. The two Cdk phosphorylation sites of PRC1 (Thr-470 and Thr-481), at the junction between the MT-binding domain and the C-terminal region, were predicted to localize closely to the N-terminal oligomerization domain.

Because the predicted PRC1 structure suggested that the CDK phosphorylation sites localize closely to the N-terminal oligomerization domain, but away from the MT-binding domain, one possibility is that phosphorylation of PRC1 by Cdk might not only control PRC1–Kif4 interaction (18), but also PRC1 MT-bundling activity, by regulating the assembly and disassembly of PRC1 oligomers. To test the possibility, we performed a series of experiments that we describe in detail below.

Cdk Phosphorylation of PRC1 Negatively Regulates PRC1 Oligomerization and Midzone Association. First, we examined whether Cdk phosphorylation affects PRC1 oligomerization. Affinity-purified goat anti-PRC1 phospho-Thr-481 antibodies (α-PRC1P) were tested for their ability to specifically recognize Cdk-phosphorylated PRC1. Bacterially expressed His-tagged PRC1 was purified and incubated with or without baculovirus-expressed purified Cdc2/cyclin B1 in the presence of ATP. The reactions were subjected to immunoblotting analysis by using anti-PRC1 antibodies (α-PRC1) or α-PRC1P. α-PRC1 recognized both Cdk-unphosphorylated and phosphorylated His-PRC1 (Fig. 1*A*). In contrast, α-PRC1P detected only Cdk-phosphorylated His-PRC1 (Fig. 1*A*). Thus, α-PRC1P specifically recognized PRC1 phosphorylated by Cdk *in vitro*. To determine whether α-PRC1P also could specifically recognize endogenous Cdk-phosphorylated PRC1, mitotic lysates of HeLa cells, which express high levels of phosphorylated PRC1 (8), were immunoprecipitated with α-PRC1. The immunoprecipitates were treated with or without purified Cdc14A or CIAP phosphatases and then subjected to immunoblotting analysis by using α-PRC1 or α-PRC1P. As shown in Fig. 1*B*, endogenous 71-kDa PRC1 was detected in immunoprecipitates treated with or without phosphatases by using α-PRC1. In contrast, CDK-phosphorylated PRC1 could be detected only in the phosphatase-untreated immunoprecipitates by using α-PRC1P. These results indicate that α-PRC1P recognizes endogenous phosphorylated PRC1 but not phosphatase-treated PRC1.

Native molecular sizes of PRC1 and phosphorylated PRC1 in

HeLa cells were determined by using sucrose gradient sedimentation, followed by immunoblotting analysis with α-PRC1 or α-PRC1P. As shown in Fig. 1*C*, α-PRC1P detected phosphorylated PRC1 only in the lower molecular mass-containing fractions corresponding to monomeric 71-kDa PRC1. In contrast, α-PRC1 detected PRC1 in two different fractions, the lower molecular mass-containing fractions corresponding to monomeric 71-kDa PRC1 and the higher molecular mass-containing fractions corresponding to oligomeric 280-kDa PRC1. Because α-PRC1 recognizes both phosphorylated and unphosphorylated PRC1, and bacterially expressed (unphosphorylated) His-PRC1 elutes from a gel-filtration column in a peak with a molecular mass of ≈300 kDa (Fig. 7, which is published as supporting information on the PNAS web site; ref. 9), we concluded that the oligomeric 280-kDa PRC1 represents unphosphorylated PRC1. In addition, we transiently expressed the N-terminal deletion mutant PRC1 protein (EYFP-PRC1ΔN184, see Fig. 5) in HeLa cells and examined the native molecular size of this mutant protein in cells by using sucrose gradient sedimentation, followed by immunoblotting analysis. Anti-GFP antibody could detect only EYFP-PRC1ΔN184 mutant protein in the low molecular mass-containing fractions, which corresponded to the monomeric form of EYFP-PRC1ΔN184 (≈80 kDa), indicating that deletion of the N-terminal oligomerization domain of PRC1 abolishes PRC1 oligomerizing activity *in vivo* (Fig. 1*C*). Taken together, these results indicate that unphosphorylated PRC1 forms oligomers (probably tetramers) via its N-terminal oligomeration domain *in vivo* and Cdk phosphorylation of PRC1 negatively affects the formation of PRC1 oligomers.

Next, we examined whether Cdk phosphorylation affects PRC1 spindle localization. HeLa cells were stained with α-PRC1P and α-PRC1. To identify spindles and DNA, cells were costained with anti-α-tubulin antibody and DAPI. As shown in Fig. 1*D*, α-PRC1P and α-PRC1 gave very similar staining patterns in early mitosis. PRC1 and phospho-PRC1 were detected on the mitotic spindle in prometaphase and metaphase. In contrast, α-PRC1P and α-PRC1 gave very different staining patterns in late mitosis. Although α-PRC1 detected PRC1 on the mitotic spindle midzone in anaphase and on the mitotic spindle midbody during cytokinesis, α-PRC1P did not detect any phosphorylated PRC1 on these spindle structures (Fig. 1*D*). These results indicate that phosphorylated PRC1 was associated with the mitotic spindle in early mitosis and that it was dephosphorylated as it translocated to the spindle midzone/midbody in anaphase and during cytokinesis.

To monitor the effects of Cdk phosphorylation on PRC1 spindle localization more directly, we performed time-lapse microscopy. HeLa cells were cotransfected with mammalian expression vectors, pEYFP-PRC1 and pECFP-histone H2B, which express an enhanced yellow fluorescent protein (EYFP)-PRC1 fusion protein and an enhanced cyan fluorescent protein (ECFP)-histone H2B fusion protein, respectively. Live cell images of transfected cells were obtained by time-lapse microscopy. Fig. 1*E* (see also Movie 2, which is published as supporting information on the PNAS web site) shows time-lapse fluorescent and phase-contrast images of HeLa cells expressing these constructs. Consistent with immunofluorescence analyses of endogenous PRC1 (Fig. 1*D*), EYFP-PRC1 associated with the mitotic spindle in early mitosis, translocated to the midzone during anaphase, and then concentrated at the midbody during cytokinesis. Like untransfected cells, cells expressing EYFP-PRC1 and ECFP-H2B progressed through mitosis and cytokinesis normally.

We coexpressed cyclin B1Δ90, a nondegradable form of cyclin B1 (21), in cells expressing EYFP-PRC1 and ECFP-H2B and examined how a constitutively active Cdc2/cyclin B1 affected PRC1 localization. Consistent with previous reports (21, 22), we found that expression of cyclin B1Δ90 in HeLa cells expressing EYFP-PRC1 and ECFP-H2B had no effects on interphase cell cycle progression, spindle formation, or chromosome alignment early in mitosis. As in control cells, EYFP-PRC1 associated with the spindle in prometaphase and metaphase (Fig. 1*F*; also see Movie 3, which is published as supporting information on the PNAS web site). However, expression of cyclin B1Δ90 in cells expressing EYFP-PRC1 and ECFP-H2B strongly affected the metaphase-to-anaphase transition and perturbed spindle dynamics, especially midzone formation and chromosome separation, ultimately resulting in failure of cytokinesis (Fig. 1*F* and Movie 3). Unlike the case in control cells, EYFP-PRC1 was found to continually localize along the entire spindle in anaphase-like cyclin B1Δ90-expressing cells. Similar perturbations of endogenous PRC1 localization also were observed in anaphase-like cyclin B1Δ90-expressing cells by using immunofluorescence analysis (Fig. 8, which is published as supporting information on the PNAS web site). α-PRC1P staining demonstrated that the spindle-associated PRC1 in anaphase-like cyclin B1Δ90-expressing cells was phosphorylated (Fig. 8). Taken together, these results demonstrate that phosphorylation of PRC1 by Cdk does not affect PRC1 association with spindle MTs but temporally controls PRC1 spindle localization, especially PRC1 association with the mitotic spindle midzone/midbody.

PRC1 is Crucial for Spindle Midzone Formation. We then determined whether midzone association of PRC1 is crucial for midzone formation. We depleted PRC1 by PRC1 small interfering RNA (siRNA) in HeLa cells or HeLa cells expressing EYFP-α-tubulin and ECFP-H2B fusion proteins. Consistent with other published results (9, 17), immunofluorescence and time-lapse microscopy analyses indicated that cells expressing undetectable levels of PRC1 displayed striking cytokinetic abnormalities (Fig. 9 and Movies 4 and 5, which are published as supporting information on the PNAS web site). We also observed striking mitotic defects in PRC1-depleted cells that have not been reported previously. Abnormal chromosome congression, misalignment, and segregation were frequently observed (Fig. 9 and Movie 5). The majority (≈80%) of cells lacking PRC1 displayed some degree of spindle disorganization, resulting in abnormal chromosome congression and misalignment in early mitosis (>300 mitotic cells were examined from three independent experiments; Fig. 9). However, immunofluorescence analysis and time-lapse video imaging revealed that cells treated with PRC1 siRNA could assemble bipolar spindles and progress from early mitosis to early anaphase even though there were some delays in the prometaphase-to-metaphase and the metaphase-to-anaphase transitions (Movie 5). These results indicated that depletion of PRC1 alone did not sufficiently perturb bipolar spindle formation and activate robust checkpoint signals to prevent anaphase onset although Cdk-phosphorylated, monomeric PRC1 that associates with spindle MTs might have a role in regulating spindle MT dynamics in early mitosis (23). We speculate that redundant factor(s), such as other microtubule-associated protein(s), might work together with PRC1 to regulate the processes in this stage of mitosis. In contrast, as PRC1 siRNA-treated cells entered anaphase, severe defects in anaphase spindle morphology were detected. The interdigitating MTs of the spindle failed to bundle, and midzone formation was not evident. Assembly of a cleavage furrow and the initiation of furrowing were observed in PRC1-depleted cells. However, the furrowing remained incomplete. Ultimately, PRC1-depleted cells failed cytokinesis and became binucleated (Fig. 9 and Movie 5).

We next explored the organization of anaphase spindles in control or PRC1-depleted cells by using 3D immunofluorescence reconstruction imaging analysis, which revealed anaphase spindle morphology and structure in remarkable detail. The anaphase spindle formed a unique, higher order, well organized, geometrical midzone structure in cells expressing PRC1 (control; Fig. 2*A*; see also Movie 6, which is published as supporting information on the PNAS web site). The antiparallel nonkinetochore interdigitating MTs bundled to form MT bundles between the separating chromosomes. As the reconstructed 3D spindle was rotated around the

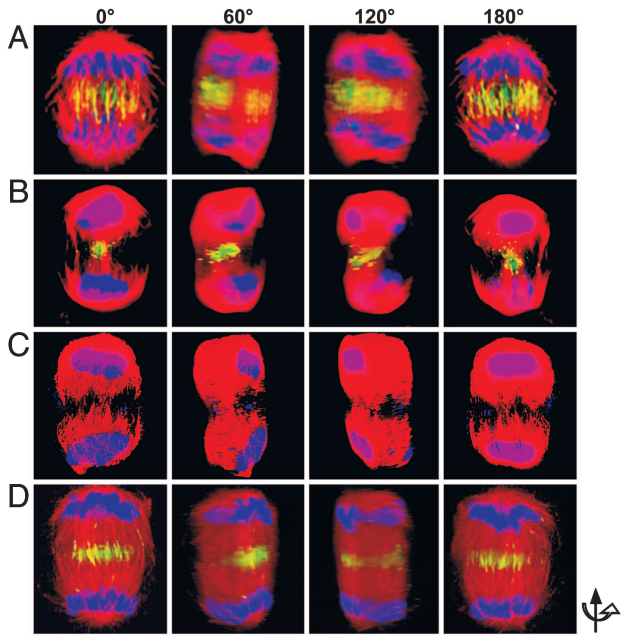

Fig. 2. Three-dimensional reconstruction images of anaphase spindle morphology and structure in a control cell, PRC1-depleted cells, and a PRC1-depleted cell expressing exogenous EYFP-PRC1ΔC. HeLa cells were transfected with control siRNA (*A*), PRC1 siRNA (*B* and *C*), or PRC1 siRNA together with pEYFP-PRC1ΔC* plasmid (*D*). Forty-eight hours after transfection, cells were fixed and stained with α-PRC1 (green in *A–C*), anti-α-tubulin antibody (red in *A–D*), and DAPI (blue in *A–D*). EYFP-PRC1ΔC is shown in green in *D*. Three-dimensional images were reconstructed from a Z-series (0.3 μm stepwise) of immunostained cells by using VOLOCITY. QUICKTIME movies of 3D images were exported according to the manufacturer's instructions. Representative images of the movies are shown.

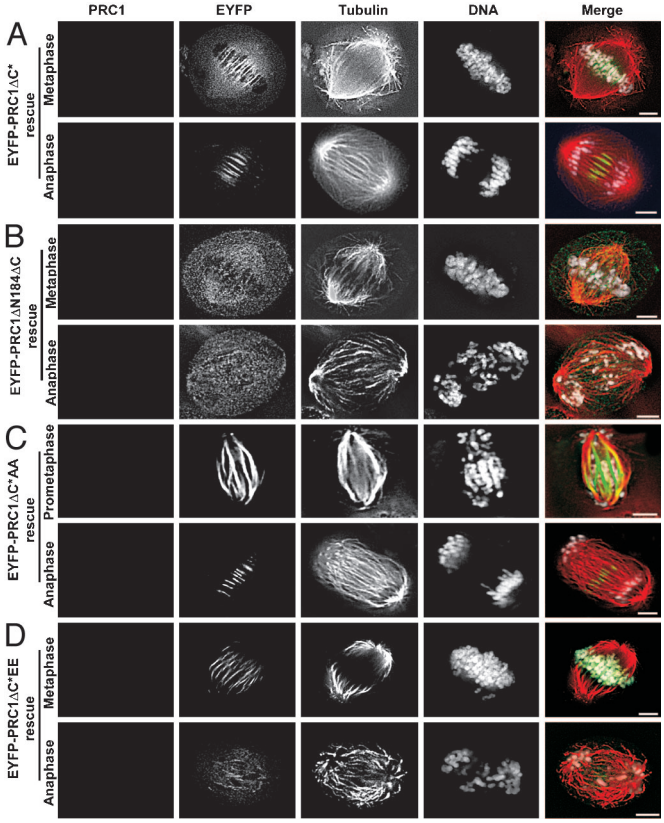

Fig. 3. The ability of ectopically expressed PRC1 oligomerization/Cdk phosphorylation mutants to rescue mitotic and cytokinetic defects, including midzone formation, in PRC1-depleted cells. HeLa cells grown on coverslips were transfected with 0.2 μg of pEYFPC1-PRC1ΔC* (*A*), pEYFPC1-PRC1ΔN184ΔC (*B*), pEYFPC1-PRC1ΔC*AA (*C*), or pEYFPC1-PRC1ΔC*EE (*D*). Twenty-four hours after transfection, cells were transfected with 100 nM PRC1 siRNA. Forty-eight hours after the second transfection, cells were fixed and stained for α-PRC1 (blue), anti-tubulin antibody (red), and DNA (white). Expression of EYFP-PRC1ΔC mutant proteins is shown in green. (Scale bars: 5 μm.)

spindle equator orthogonally, the spatial colocalization of PRC1 with the midzone MT bundles could be visualized clearly (Movie 6). PRC1 virtually colocalized with every midzone MT bundle. However, PRC1 did not colocalize with unbundled astral MTs.

The 3D analysis revealed that PRC1-depleted cells displayed aberrant anaphase spindle morphology, with especially severe abnormalities in the midzone. The degree of midzone abnormality correlated with the reduction of PRC1 expression (Fig. 2 *B* and *C*; see also Movies 7 and 8, which are published as supporting information on the PNAS web site). Cells expressing reduced levels of PRC1 showed formation of a poorly organized and disarrayed spindle midzone (Fig. 2*B* and Movie 7). Interdigitating MT bundles were observed only in areas where PRC1 was present. In the absence of PRC1, MTs were unbundled and dispersed. In cells expressing undetectable levels of PRC1, no interdigitating MT bundles were detected (Fig. 2*C* and Movie 8). The interpolar MTs were completely disarrayed and dispersed. As a result, the spindle broke into two abnormal half spindles. Lagging chromosomes were clearly visible in the PRC1-depleted cells, confirming a role of PRC1 in chromosome segregation.

If PRC1 is essential for midzone formation, then expression of exogenous PRC1 should reestablish the midzone in PRC1-depleted cells. Therefore, we performed rescue experiments with pEYFP-PRC1ΔC*, a mammalian expression plasmid that fuses EYFP to a mutant PRC1 cDNA (with silent mutations in the region targeted by our PRC1 siRNA and a 105-bp deletion in its 3′ coding region). PRC1 siRNA thus would silence the expression of endogenous PRC1, but not EYFP-PRC1ΔC, when cotransfected into cells. The fusion of EYFP to PRC1ΔC also allowed us to discriminate between endogenous PRC1 and exogenous EYFP-PRC1. Previous studies showed that the EYFP-PRC1ΔC fusion protein, which contains a 35-aa truncation at the PRC1 C terminus, is fully functional and displays the same subcellular localization and function as WT PRC1 protein during mitosis (9). However, unlike the full-length PRC1 protein, EYFP-PRC1ΔC could not be recognized by α-PRC1, which was raised against the last 20 amino acids of PRC1 (8).

HeLa cells were cotransfected with PRC1 siRNA and pEYFP-PRC1ΔC*, and immunoblotting and immunofluorescence staining analyses revealed that PRC1 siRNA could effectively ablate the expression of endogenous PRC1 but not EYFP-PRC1ΔC (Fig. 10, which is published as supporting information on the PNAS web site). Expression of EYFP-PRC1ΔC in cells lacking endogenous PRC1 rescued virtually all mitotic and cytokinetic defects, including abnormal spindle morphology and aberrant chromosome segregation, and also the defect in cytokinesis observed in cells that were only depleted of endogenous PRC1 (see below and Fig. 3). Three-dimensional reconstruction imaging analysis indicated that the interdigitating MTs were rebundled and that the midzone was reestablished in the presence of EYFP-PRC1ΔC in endogenous PRC1-depleted cells (Figs. 2*D* and 10; see also Movie 9, which is published as supporting information on the PNAS web site). Thus, EYFP-PRC1ΔC compensated for the depletion of endogenous PRC1. These results, together with the previous results that PRC1 has MT-binding and -bundling activities (9), demonstrated that

PRC1 is essential for bundling interdigitating MTs to form the midzone in mammalian cells.

Essential Role of Oligomerization/Cdk Dephosphorylation of PRC1 in Midzone Formation. Next, we examined the role of Cdk dephosphorylation and PRC1 oligomerization in regulating midzone formation. We performed rescue experiments similar to those described above by using PRC1 oligomerization/phosphorylation mutant proteins (see Figs. 5, 6, and 10*A*; see also Fig. 11, which is published as supporting information on the PNAS web site). HeLa cells were cotransfected with PRC1 siRNA together with a mammalian expression vector expressing EYFP-PRC1ΔC, EYFP-PRC1ΔN184ΔC (a mutant in which the oligomerization domain of PRC1 was deleted), EYFP-PRC1ΔCAA (a nonphosphorylatable mutant in which the Cdk phosphorylation sites Thr-470 and Thr-481 were substituted by alanines), or EYFP-PRC1ΔCEE (a phosphomimetic mutant in which the Cdk phosphorylation sites were substituted with glutamates) (Fig. 10*A*). Immunofluorescence analyses indicated that expression of EYFP-PRC1ΔC, but not nonoligomerizable mutant EYFP-PRC1ΔN184ΔC or phosphomimetic mutant EYFP-PRC1ΔCEE, rescued the mitotic and cytokinetic defects in endogenous PRC1-depleted cells (Figs. 3 *A*, *B*, and *D* and 10*C*). Like untransfected cells, cells expressing EYFP-PRC1ΔC but lacking endogenous PRC1 ($n = 150$) displayed normal mitotic spindle assembly, especially midzone formation, chromosome congression, alignment, and segregation, and completion of cytokinesis. Like endogenous PRC1, EYFP-PRC1ΔC localized to mitotic spindles in early mitosis and then to midzone/midbody interdigitating MT bundles in late mitosis and cytokinesis (Fig. 3*A*).

In contrast, cells lacking endogenous PRC1 but expressing EYFP-PRC1ΔN184ΔC ($n = 106$) or EYFP-PRC1ΔCEE ($n = 124$) still displayed abnormal mitotic spindle and midzone formation, aberrant chromosome congression, alignment and segregation, and cytokinesis failure. Formation of the midzone-interdigitating MT bundles was not evident in any anaphase-like PRC1-depleted, EYFP-PRC1ΔN184ΔC- or EYFP-PRC1ΔCEE-expressing cells (Fig. 3 *B* and *D*). EYFP-PRC1ΔN184ΔC or EYFP-PRC1ΔCEE continually localized along the entire mitotic spindle. These results indicate that the expression of EYFP-PRC1ΔN184ΔC or EYFP-PRC1ΔCEE cannot compensate for the depletion of endogenous PRC1 in these cells. Of particular note, the abnormalities of chromosome segregation and midzone formation observed in anaphase-like PRC1-depleted EYFP-PRC1ΔCEE-expressing cells were very similar to those observed in anaphase-like cells expressing Δ90 cyclin B1 (Figs. 3*D* and 8).

Cells expressing Cdk-nonphosphorylatable mutant EYFP-PRC1ΔCAA but lacking endogenous PRC1 ($n = 123$) revealed more complex phenotypes (Figs. 3*C* and 10*C*). In cells expressing high levels EYFP-PRC1ΔCAA without endogenous PRC1, mitotic spindle MTs bundled extensively in early mitosis, resulting in the formation of abnormal spindle morphology, aberrant chromosome congression and alignment, and mitotic arrest (Fig. 3*C Upper*). The phenotypes observed in these cells were similar to those in cells overexpressing the EGFP-PRC1AA mutant reported in ref. 9. In contrast, cells expressing low levels of EYFP-PRC1ΔCAA rescued the mitotic and cytokinetic defects in endogenous PRC1-depleted cells. In these cells, normal chromosome segregation was restored, the midzone was reestablished, and EYFP-PRC1ΔCAA colocalized with interdigitating MT bundles (Fig. 3*C Lower*).

Thus, the results obtained from these rescue experiments demonstrate that Cdk dephosphorylation/oligomerization of PRC1 plays an essential role in regulating the bundling of midzone interdigitating MT bundles, chromosome segregation, and cytokinesis.

Interdigitating MT Bundles Were Observed in Kif4-Depleted Cells. Finally, we determined whether Kif4 is required for PRC1 bundling of interdigitating MTs. HeLa cells were transfected with Kif4 siRNA to deplete endogenous Kif4 as described in ref. 18 (see also Fig. 12, which is published as supporting information on the PNAS web site). Transfected cells were immunostained with α-PRC1P and α-PRC1. To localize the spindle and DNA, cells were costained with anti-α-tubulin antibody and DAPI. Consistent with our published results (18), cells transfected with Kif4 siRNA did not show any detectable mitotic defects in early mitosis, and PRC1 was phosphorylated and localized to the mitotic spindle (Fig. 4*A*). In contrast, cells transfected with Kif4 siRNA displayed striking mitotic and cytokinetic defects, including abnormalities of PRC1 localization in late mitosis and cytokinesis. In Kif4 siRNA-treated anaphase/telophase-like cells, the spindle elongated extensively with the bundled interdigitating MTs in between separating chromosomes. Because PRC1 could not be translocated to the plus ends of interdigitating MTs in the absence of Kif4, formation of the well organized midzone/midbody was not evident. However, in these cells, PRC1 was dephosphorylated and colocalized with the elongated interpolar spindle bundles (Fig. 4*A*). Because dephosphorylated PRC1 is crucial for bundling the interdigitating MTs, we concluded that bundling of interdigitating MTs by PRC1 does not require Kif4. However, we cannot exclude the possibility that very low levels of Kif4 (beyond the detection limits of immunofluorescence) might be sufficient to participate in MT bundling with PRC1.

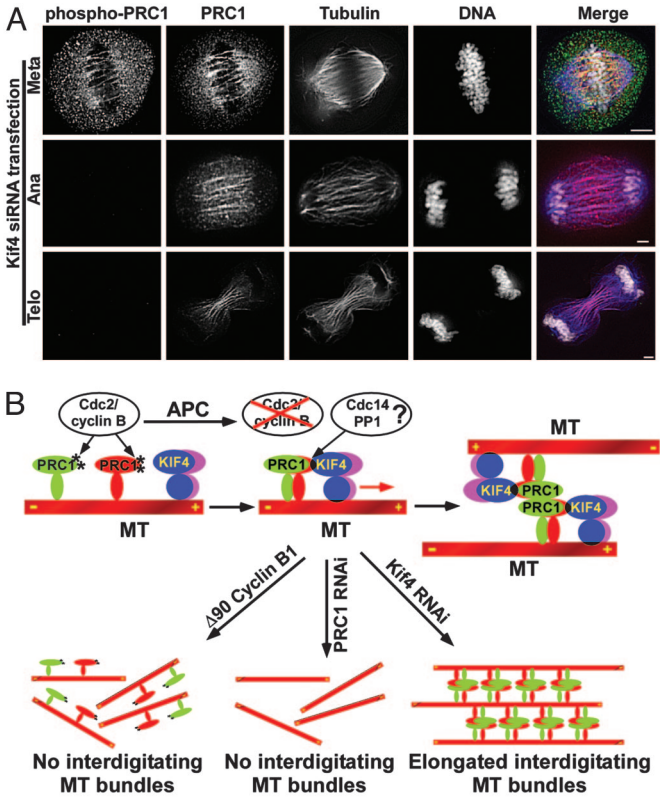

Fig. 4. Interdigitating MT bundles in Kif4 siRNA-treated cells. (*A*) HeLa cells grown on coverslips were transfected with 100 nM Kif4 siRNA as described in ref. 18. Two days after transfection, cells were fixed and stained with α-PRC1P (green), α-PRC1 (red), anti-α-tubulin antibody (blue), and DAPI (DNA, white). (Scale bars: 5 μm.) (*B*) The proposed model for temporal and spatial control of midzone formation by PRC1 in mammalian cells (see text for details).

Taken together, our results demonstrate that PRC1 is an essential factor required for controlling the spatial and temporal formation of the midzone in human cells. In addition to the fact that Cdk phosphorylation controls PRC1 interaction with Kif4 and the translocation of PRC1 along mitotic spindles to the plus ends of interdigitating MTs (18), we now show that Cdk phosphorylation also controls PRC1 MT-bundling activity by regulating the assem-

bly and disassembly of PRC1 oligomers. We provide direct evidence that oligomerization/Cdk phosphorylation plays an essential role in regulating PRC1's MT-bundling function that is necessary for midzone formation. Based on our findings, together with published results in refs. 9 and 18, we present the following model for spatial and temporal control of midzone formation by PRC1 in human cells (Fig. 4*B*). Cdk (mainly Cdc2/cyclin B) phosphorylates PRC1 in early mitosis. However, this modification does not affect PRC1 binding to spindle MTs but instead holds it in a monomeric state to prevent PRC1 MT-bundling activity. MT-bound, Cdk-phosphorylated, monomeric PRC1 also cannot interact with Kif4 on the spindle. During the metaphase-to-anaphase transition, when all cellular Cdk activity is eliminated because of APC-mediated degradation of cyclin B, PRC1 is dephosphorylated by an active mitotic phosphatase (e.g., Cdc14A or PP1γ). Dephosphorylation promotes PRC1's interaction with Kif4, which then translocates PRC1 along mitotic spindles to the plus ends of antiparallel interdigitating MTs. In addition, dephosphorylation of PRC1 promotes its MT-bundling activity by promoting its oligomerization. Thus, the plus end-associated, dephosphorylated PRC1 proteins bundle the antiparallel interdigitating MTs to form the midzone, which serves a platform, or "landing pad," for the localization of other critical spindle midzone-associated proteins, such as the centralspindlin and chromosomal passenger proteins that are involved in regulating the final cell division process, cytokinesis (refs. 16 and 17; C.Z. and W.J., unpublished results). Future studies in this area should focus on identifying the protein phosphatase(s) required for dephosphorylation of PRC1 during the metaphase-to-anaphase transition.

Materials and Methods

Antibodies, Plasmids, and siRNA Oligonucleotides. Rabbit anti-PRC1 antibodies (α-PRC1) generated against a PRC1 C-terminal peptide (amino acids 601–620) were described in ref. 8. Goat anti-PRC1 phospho-Thr-481 antibodies (α-PRC1P) were purchased from Santa Cruz Biotechnology. Mouse monoclonal anti-tubulin antibody was obtained from Sigma. All secondary antibodies were purchased from Jackson ImmunoResearch.

Human PRC1 cDNA and its deletion mutants (see Fig. 5) were generated by PCR and subcloned into EcoRI/XhoI sites of pFLAG, pCS3, or pEYFP-C1 plasmid. pEYFP-PRC1ΔC*, pEYFP-PRC1ΔCAA*, or pEYFP-PRC1ΔCEE*, in which PRC1 siRNA target sequences (AAGGGATTCCAGAGGACCA) were mutated to (AAGGAATCCCGGAAGATCA) or Cdk phosphorylation sites, Thr-470 and Thr-481, were substituted to Ala or Glu, were generated by QuikChange mutagenesis method according to the manufacturer's description (Stratagene). Human cyclin B1Δ90 cDNA was generated by PCR and subcloned into BglII/SalI sites of pEGFP-C1 plasmid. All constructs were fully sequenced. pEYFP-tubulin and pECFP-histone H2B were described in ref. 7.

siRNAs were synthesized by Dharmacon Research (Lafayette, CO). RNA oligonucleotide sequences used for targeting PRC1 were (AA)GGGAUUCCAGAGGACCA (nucleotides 86–104). Scrambled siRNA used as a control was purchased from Dharmacon Research.

Cell Culture, Transfection, Immunoprecipitation, Immunoblotting, and Immunofluorescence Analyses. HeLa cells were cultured in DMEM supplemented with 10% FBS at 37°C and 5% CO_2 in a humidified incubator. Cell transfection, immunoprecipitation, immunoblotting, and immunofluorescence analyses was performed as described in ref. 7. For rescue experiments, HeLa cells were seeded in 6- to 24-well plates in DMEM plus 10% FBS overnight and then transfected with 0.2–0.5 μg of plasmids by using Lipofectamine 2000 (Invitrogen). One day after transfection, cells were transfected with a 100 nM concentration of control or PRC1 siRNA by using Oligofectamine (Invitrogen). Two days after the second transfection, cells were lysed or fixed for immunoblotting or immunofluorescence analysis.

Time-Lapse Microscopy. HeLa cells grown on a 35-mm polylysine-coated glass-bottom microwell dish (MatTek, Ashland, MA) were transfected with mammalian expression plasmids and/or siRNA by using Lipofectamine 2000 or Oligofectamine (Invitrogen). One day after transfection, cells were changed into CO_2 independent medium (GIBCO) containing 10% FBS overnight. Dishes were then covered with mineral oil (Sigma) and transferred to a heated stage (37°C) on an inverted Zeiss Axiovert 100M microscope. Phase-contrast and fluorescence images of live cells were collected at 2-min intervals for 9–10 h. Movie images were collected and processed by using SLIDEBOOK 3.0 (Intelligent Imaging Innovations, Santa Monica, CA) and exported as QUICKTIME (Apple Computer, Cupertino, CA) movies (7).

Three-Dimensional Reconstruction Imaging Analysis. Serial thin sections (0.3 μm) of immunofluorescent stained cells were scanned under a ×63 oil objective by using an inverted Leica DMIRE2 microscope. Images were imported into the library of Volocity (Improvision, Lexington, MA) and rendered to 3D volume. The 3D images were generated by using VOLOCITY software and exported as QUICKTIME movies.

We thank Drs. Nanxin Li, Joel Leverson, and Gary Chiang for critical reading of the manuscript; Dr. Nick Wells for helping to determine the oligomerization domain of PRC1; and Ningning Sai for laboratory support. E.L. was supported by National Institutes of Health Predoctoral Fellowship 2T32 CA77109-06A2. This work was supported by grants from the Edward Mallinckrodt, Jr. Foundation and the Lisa U. Pardee Foundation and National Institutes of Health Grant GM67859 (to W.J.).

1. D'Avino, P. P., Savoian, M. S. & Glover, D. M. (2005) *J. Cell Sci.* **118,** 1549–1558.
2. McCollum, D. (2004) *Curr. Biol.* **14,** R953–R955.
3. Mishima, M., Kaitna, S. & Glotzer, M. (2002) *Dev. Cell* **2,** 41–54.
4. Mishima, M., Pavicic, V., Gruneberg, U., Nigg, E. A. & Glotzer, M. (2004) *Nature* **430,** 908–913.
5. Bowerman, B. (2004) *Nature* **430,** 840–842.
6. Matuliene, J. & Kuriyama, R. (2004) *Mol. Biol. Cell* **15,** 3083–3094.
7. Zhu, C., Bossy-Wetzel, E. & Jiang, W. (2005) *Biochem. J.* **389,** 373–381.
8. Jiang, W., Jimenez, G., Wells, N. J., Hope, T. J., Wahl, G. M., Hunter, T. & Fukunaga, R. (1998) *Mol. Cell* **2,** 877–885.
9. Mollinari, C., Kleman, J. P., Jiang, W., Schoehn, G., Hunter, T. & Margolis, R. L. (2002) *J. Cell Biol.* **157,** 1175–1186.
10. Schuyler, S. C., Liu, J. Y. & Pellman, D. (2003) *J. Cell Biol.* **160,** 517–528.
11. Verni, F., Somma, M. P., Gunsalus, K. C., Bonaccorsi, S., Belloni, G., Goldberg, M. L. & Gatti, M. (2004) *Curr. Biol.* **14,** 1569–1575.
12. Verbrugghe, K. J. & White, J. G. (2004) *Curr. Biol.* **14,** 1755–1760.
13. Loiodice, I., Staub, J., Setty, T. G., Nguyen, N. P., Paoletti, A. & Tran, P. T. (2005) *Mol. Biol. Cell* **16,** 1756–1768.
14. Yamashita, A., Sato, M., Fujita, A., Yamamoto, M. & Toda, T. (2005) *Mol. Biol. Cell* **16,** 1378–1395.
15. Chang, H. Y., Smertenko, A. P., Igarashi, H., Dixon, D. P. & Hussey, P. J. (2005) *J. Cell Sci.* **118,** 3195–3201.
16. Kurasawa, Y., Earnshaw, W. C., Mochizuki, Y., Dohmae, N. & Todokoro, K. (2004) *EMBO J.* **23,** 3237–3248.
17. Mollinari, C., Kleman, J. P., Saoudi, Y., Jablonski, S. A., Perard, J., Yen, T. J. & Margolis, R. L. (2005) *Mol. Biol. Cell* **16,** 1043–1055.
18. Zhu, C. & Jiang, W. (2005) *Proc. Natl. Acad. Sci. USA* **102,** 343–348.
19. Jaroszewski, L., Li, W. & Godzik, A. (2002) *Protein Sci.* **11,** 1702–1713.
20. Soelaiman, S., Jakes, K., Wu, N., Li, C. & Shoham, M. (2001) *Mol. Cell* **8,** 1053–1062.
21. Clute, P. & Pines, J. (1999) *Nat. Cell Biol.* **1,** 82–87.
22. Wheatley, S. P., Hinchcliffe, E. H., Glotzer, M., Hyman, A. A., Sluder, G. & Wang, Y. (1997) *J. Cell Biol.* **138,** 385–393.
23. Ban, R., Irino, Y., Fukami, K. & Tanaka, H. (2004) *J. Biol. Chem.* **279,** 16394–16402.